Chirp Signal Transmission and Reception With Orbital Angular Momentum Multiplexing

Gaofeng Shu, Wentao Wang, Da Liang, Yunkai Deng, *Member, IEEE*, Robert Wang, *Senior Member, IEEE*, Heng Zhang, and Ning Li, *Member, IEEE*

***Abstract*—Vortex electromagnetic waves, which carry the orbital angular momentum (OAM), can increase channel capacity by utilizing OAM multiplexing technology in optical field. In order to fully exploit OAM mode-division multiplexing in radio domain, a crosstalk matrix of the communication channel between the multi-OAM-mode transmission and reception is deduced theoretically in this letter. The crosstalk matrix shows that it is achievable to communicate between the same OAM modes but not possible between different OAM modes. To confirm this statement, a near-field proof-of-concept communication experiment, transmitting and receiving linear frequency modulation signals with different frequency modulation (FM) rate using uniform circular array antenna, is then carried out. The experimental results show that the crosstalk between different modes meets the requirements of near-field communication. It may also be beneficial for the application of the vortex wave for radar imaging in the future.**

***Index Terms*—Chirp signal, multiplexing and demultiplexing, near-field communication, orbital angular momentum (OAM), radio, vortex waves.**

I. Introduction

IT IS WELL known that an electromagnetic (EM) system can radiate linear momentum and angular momentum into far zone. In 1992, Allen *et al.* [1] found that an orbital angular momentum (OAM) was defined well in a Laguerre–Gaussian laser mode. Analogously, OAM in radio can also induce a suspended torsion pendulum to rotate [2]. An EM wave or light beam carrying OAM also called vortex or vorticity [3]–[6] has helical phase wavefront of $e^{jL\phi}$, where ϕ is the transverse azimuthal angle and L is an integer indicating the topological charge. According to the peculiar phase properties of vortex waves, vortex beam has a singularity along the beam axis, and the main lobe diffuses outward as the distance increases.

Manuscript received February 17, 2019; revised March 19, 2019; accepted March 19, 2019. Date of publication March 25, 2019; date of current version May 3, 2019. This work was supported in part by the National Natural Key R&D Program of China under Contract 2017YFB0502700 and in part by the National Natural Science Foundation of China under Contract 61422113. *(Corresponding author: Robert Wang.)*

G. Shu and D. Liang are with the Spaceborne Microwave Remote Sensing System Department, Institute of Electronics, Chinese Academy of Sciences, Beijing 100190, China, and also with the University of Chinese Academy of Sciences, Beijing 100039, China (e-mail: gaofeng.shu@foxmail.com; daliang16@foxmail.com).

W. Wang, Y. Deng, R. Wang, H. Zhang, and N. Li are with the Department of Spaceborne Microwave Remote Sensing System, Institute of Electronics, Chinese Academy of Sciences, Beijing 100190, China (e-mail: wwt_iecas@163.com; ykdeng@mail.ie.ac.cn; yuwang@mail.ie.ac.cn; caszhmail@163.com; lining_nuaa@163.com).

Digital Object Identifier 10.1109/LAWP.2019.2906996

In contrast to the OAM being fully utilized for communications in the optical frequency range [7]–[10], OAM has so far not been used to its full extent in the radio domain, except for some simulations and proof-of-concept experiments. Numerical simulations of generating radio beams with OAM were first performed by Thidé *et al.* [11] in 2007, which set off a very interesting wave of research works on the OAM in radio frequencies. Radio beams carrying the OAM can be easily generated, transmitted, and measured via laboratory experiments [12]. In 2012, Tamburini *et al.* carried out an experiment of information transmission with radio vorticity encoding multichannel on the same frequency in outdoor environment [13]. The results showed that different OAM states of EM waves within the same frequency bandwidth are orthogonal to each other in free space and can be detected far away from transmitting antennas. A series of experiments were described in [14] and [15] demonstrating that it is feasible and compatible to utilize OAM beams as the carrier of data transport or channel multiplexing.

In order to further exploit the high capacity of OAM mode-division multiplexing in radio domain, a near-field communication experiment with OAM multiplexing inspired by [16] and [17] is conducted in this letter. It is supposed to show that different communication channels based on radio OAM are mutually orthogonal in free space and each channel can carry completely different information on the same bandwidth. To fulfill this purpose, we generate and multiplex three radio vortices with different L values carrying chirp signals with different bandwidth on *X*-band by using concentric uniform circular arrays (UCAs) composed by back-fed horn antennas reformed from the work presented in [18] as transmitter (TX). All three beams were sampled by receiver (RX), the identical arrays placed at a short distance from the TX in line of sight (LOS). Then, the crosstalk of OAM channels is analyzed, and the received data are recovered.

This letter is organized as follows. In Section II, we build a generic model of our experiment configuration and then briefly derive transfer function of the system, which helps us investigate how signals behave from TX to RX. Several experiments are described in Section III, i.e., generating radio OAM waves, transmission and reception of single-frequency signals and linear frequency modulation (LFM, chirp) signals, and radio OAM multiplexing and demultiplexing. Conclusions are drawn in Section IV.

II. Basic Theory Analysis

A. Formulas of the Model

In this section, a brief introduction of the experimental configuration, which consists of several subsystems, is first given.

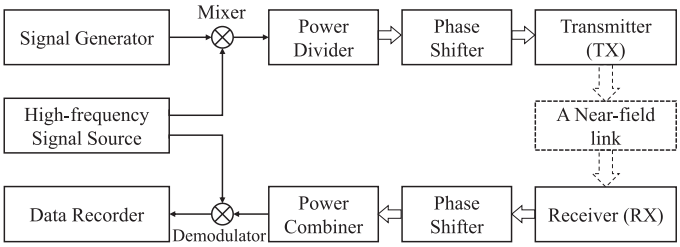

Fig. 1. Schematic diagram of one channel of the communication link based on radio OAM multiplexing.

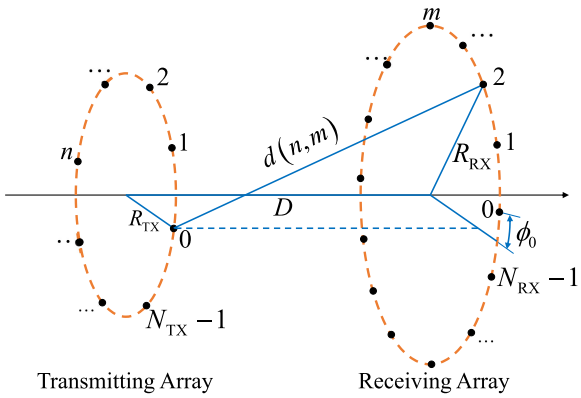

Fig. 2. Diagram of two UCAs configuration. The two planes of UCAs are parallel.

Subsequently, some formulas related to the system are deduced. The experimental setup is shown. Fig. 1 demonstrates one channel of our multiplexing system.

Let signals generated by signal generator at the end of each output of power divider be s. The process of phase shifting can be expressed mathematically as follows:

$$\boldsymbol{t}_{\mathrm{TX}} = \left[\mathrm{e}^{\mathrm{j}\phi_{\mathrm{TX},0}}, \mathrm{e}^{\mathrm{j}\phi_{\mathrm{TX},1}}, \ldots, \mathrm{e}^{\mathrm{j}\phi_{\mathrm{TX},N_{\mathrm{TX}}-1}}\right] \tag{1}$$

where $\phi_{\mathrm{TX},n} = 2\pi L_{\mathrm{TX}} n / N_{\mathrm{TX}}$ $(n = 0, 1, \ldots, N_{\mathrm{TX}} - 1)$, L_{TX} is transmitting OAM mode, and N_{TX} denotes the number of output ports of power divider. Obviously, regarding power divider and phase shifter as a system, the signals at the end of TX can be expressed as

$$\boldsymbol{s}_t = s \cdot \boldsymbol{t}_{\mathrm{TX}}. \tag{2}$$

Due to power divider, the signal s is split into N_{TX} signals, i.e., $\boldsymbol{s}_t$. Generally in this letter, bold lowercase letters indicate vectors and bold uppercase letters denote matrices.

In light of the most general situation, we consider two UCAs, where one consists of N_{TX} elements and the other one N_{RX}, as shown in Fig. 2. The black solid dots represent the position of the antenna elements, and each element is numbered.

Let the distance between TX and RX be D, and their radii are R_{TX} and R_{RX}, respectively. The angle between first elements in the two arrays is denoted as ϕ_0. According to the geometric configuration, the distance between nth element in TX and mth element in RX is

$$d(n,m) = \sqrt{D^2 + R_{\mathrm{TX}}^2 + R_{\mathrm{RX}}^2 - 2R_{\mathrm{TX}}R_{\mathrm{RX}}\cos(\Delta\phi_{n,m})} \tag{3}$$

where $\Delta\phi_{n,m} = \frac{2\pi n}{N_{\mathrm{TX}}} - \frac{2\pi m}{N_{\mathrm{RX}}} + \phi_0$ is the central angle of the projection of the two elements on the array plane.

Now, let us investigate arbitrary two antennas with a distance of r in free space. The electric field components everywhere around a short dipole placed along z-axis and with its center at the origin in spherical coordinate system are

$$\begin{cases} E_r = \dfrac{I_0 L k^2 \cos\theta\, \mathrm{e}^{-\mathrm{j}kr}}{2\pi\varepsilon_0 c_0}\left(\dfrac{1}{k^2r^2} + \dfrac{1}{\mathrm{j}k^3r^3}\right) \\ E_\theta = \dfrac{I_0 L k^3 \sin\theta\, \mathrm{e}^{-\mathrm{j}kr}}{4\pi\omega\varepsilon_0}\left(\dfrac{\mathrm{j}}{kr} + \dfrac{1}{k^2r^2} + \dfrac{1}{\mathrm{j}k^3r^3}\right) \end{cases} \tag{4}$$

using the notation in [19].

In our experiment, RX is placed in radiating near-field (Fresnel) region, i.e., $r < 2A^2/\lambda$, where A is the total aperture of TX and RX. However, the distance between TX and RX satisfies $kr \approx 321.7 \gg 1$. The terms including $1/(kr)^2$ and $1/(kr)^3$ in (4) can thus be neglected in favor of the terms in $1/(kr)$, hence the transfer function from transmitting antenna to receiving antenna then can be written as

$$h(r) = \beta\frac{1}{4\pi r\lambda}\,\mathrm{e}^{-\mathrm{j}kr} \tag{5}$$

where β is normalized factor. Substituting (3) into (5) and representing $h(d(n,m))$ as $h_{n,m}$, the transfer matrix from TX and RX can be expressed as

$$\boldsymbol{H} = \begin{bmatrix} h_{0,0} & h_{0,1} & \cdots & h_{0,N_{\mathrm{RX}}-1} \\ h_{1,0} & h_{1,1} & \cdots & h_{1,N_{\mathrm{RX}}-1} \\ \vdots & \vdots & \ddots & \vdots \\ h_{N_{\mathrm{TX}}-1,0} & h_{N_{\mathrm{TX}}-1,1} & \cdots & h_{N_{\mathrm{TX}}-1,N_{\mathrm{RX}}-1} \end{bmatrix}. \tag{6}$$

Consequently, the signals RX received are

$$\boldsymbol{s}_r = \boldsymbol{s}_t\boldsymbol{H}. \tag{7}$$

The process of phase shifting at receiving end is

$$\boldsymbol{t}_{\mathrm{RX}} = \left[\mathrm{e}^{\mathrm{j}\phi_{\mathrm{RX},0}}, \mathrm{e}^{\mathrm{j}\phi_{\mathrm{RX},1}}, \ldots, \mathrm{e}^{\mathrm{j}\phi_{\mathrm{RX},N_{\mathrm{RX}}-1}}\right]^{\mathrm{H}} \tag{8}$$

where $\phi_{\mathrm{RX},m} = 2\pi L_{\mathrm{RX}} m / N_{\mathrm{RX}}$ $(m = 0, 1, \ldots, N_{\mathrm{RX}} - 1)$ and $[\cdot]^{\mathrm{H}}$ denotes conjugate transpose or Hermitian transpose. The synthesized signal then has the following form:

$$s_s = \boldsymbol{s}_r\boldsymbol{t}_{\mathrm{RX}} = s\boldsymbol{t}_{\mathrm{TX}}\boldsymbol{H}\boldsymbol{t}_{\mathrm{RX}} \tag{9}$$

where subscript s in s_s means "synthesized" and the N_{RX} signals $\boldsymbol{s}_r$ thus become one signal s_s, which is different from the initial signal s.

B. OAM Multiplexing and Demultiplexing Analysis

In order to understand the relationship between s_s and s, let us define

$$\sigma = \boldsymbol{t}_{\mathrm{TX}}\boldsymbol{H}\boldsymbol{t}_{\mathrm{RX}} \tag{10}$$

which is called the transformation factor, and thus $s_s = s\sigma$. Obviously, σ is determined by the system parameters, such as the number of antenna elements, the distance of TX and RX, etc. According to (1), (6), and (8) and ignoring the amplitude factor, it is not difficult to get

$$\sigma = \begin{cases} \sigma_{L_{\mathrm{TX}},L_{\mathrm{RX}}}, & \text{if } L_{\mathrm{TX}} = L_{\mathrm{RX}} \\ 0, & \text{if } L_{\mathrm{TX}} \neq L_{\mathrm{RX}} \end{cases} \tag{11}$$

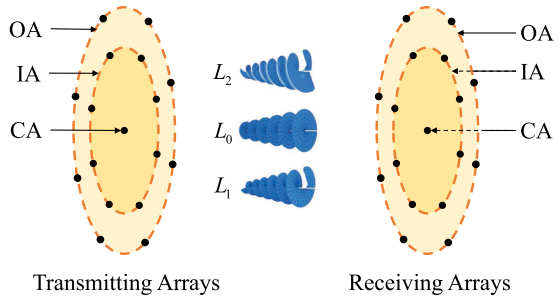

Fig. 3. Diagram of TX and RX. CA: central antenna; IA: inner array; OA: outer array.

where $\sigma_{L_{\mathrm{TX}},L_{\mathrm{RX}}}$ is complex, nonzero, and strongly related to system parameters. The subscript indicates the OAM mode of transmitting and receiving.

Given that a special antenna configuration shown in Fig. 3 consists of a single central antenna and two concentric UCAs. Then, three OAM beams with three different modes are generated and copropagate in free space from TX to RX.

According to (11), transformation factor matrix of the antenna configuration can be expressed as following:

$$\boldsymbol{\Sigma} = \begin{bmatrix} \sigma_{0,0} & \sigma_{0,1} & \sigma_{0,2} \\ \sigma_{1,0} & \sigma_{1,1} & \sigma_{1,2} \\ \sigma_{2,0} & \sigma_{2,1} & \sigma_{2,2} \end{bmatrix} = \begin{bmatrix} \sigma_{0,0} & 0 & 0 \\ 0 & \sigma_{1,1} & 0 \\ 0 & 0 & \sigma_{2,2} \end{bmatrix} \tag{12}$$

where $\boldsymbol{\Sigma}$ is a diagonal matrix, where diagonal elements are nonzero, and zero otherwise. It must be stated that the effects of noise are ignored in all the previous analyses. For practical needs, we define an indicator, named "relative average crosstalk (RAC)" and denoted by $\mathcal{C}$, to evaluate crosstalk of the system, i.e.,

$$\mathcal{C} = 20\log_{10}\left(\frac{\sum_{i\neq j}\boldsymbol{\Sigma}/6}{\sum_{i=j}\boldsymbol{\Sigma}/3}\right). \tag{13}$$

Obviously, if there is no noise, $\mathcal{C} = -\infty$. Furthermore, the smaller $\mathcal{C}$ is, the lower RAC is, hence the better communication performance is.

If the signals radiated by TX are $\boldsymbol{s}_g = [s_0, s_1, s_2]$, then signals received by RX become

$$\boldsymbol{s}_v = \boldsymbol{s}_g\boldsymbol{\Sigma} = [s_0\sigma_{0,0}, s_1\sigma_{1,1}, s_2\sigma_{2,2}]. \tag{14}$$

As it can be seen from (14), when s_0, s_1, and s_2 carry different information, they can be received and distinguished simultaneously via configuring different receiving strategies. After a simple analysis mentioned earlier, it is straightforward to show that the whole proposed system can demultiplex transmitted signals based on OAM multiplexing in hardware level rather than software level. In Section III, some experiments were conducted based on chirp signals on *X*-band, which are widely used waveforms in radar field.

III. Experiments

A. Experimental Setup

In our experiment, as shown in Fig. 1, the chirp signals are generated by means of arbitrary waveform generator (AWG), modulated by mixer to *X*-band and divided into multiple signals with equal power by power divider. To generate the desired

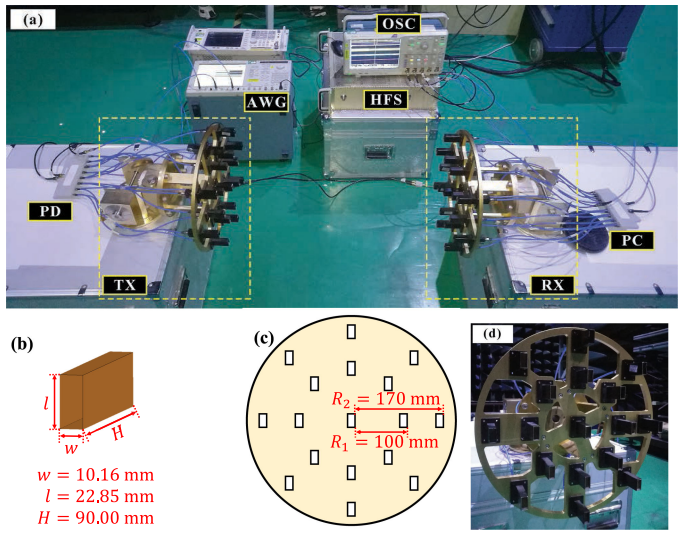

Fig. 4. (a) Photograph of the experimental setup. TX and RX in the picture were placed closer to each other for photographing conveniently. AWG: Arbitrary waveform generator; HFS: High-frequency source; OSC: Oscilloscope; PD: power divider; PC: power combiner. (b) Antenna element and its size parameters. (c) Elements configuration of TX and RX. (d) Photograph of TX.

OAM mode, the phase shifter delays each adjacent signal with a particular phase, 45° for $L = 1$, 90° for $L = 2$, etc. EM vortices carrying different OAM modes are radiated into free space via TX, and then inducted by RX. The elements of TX and RX are back-fed rectangle waveguides with height of 90.00 mm, length of 22.86 mm, and width of 10.16 mm, which are operated at *X*-band with 40% relative bandwidth, horizontal polarization, and sidelobe level of -1.86 dB. Using phase shifter, we shift phases of received signals with $-L$ mode to "grasp" the desired OAM mode. After demodulation, the signal is recorded by the data acquisition recorder, such as a high sampling rate oscilloscope. The experimental configuration is shown in Fig. 4.

Different lengths of coaxial cables with SMA connector are applied to implement phase shifting. The operating frequency of the coaxial cables is 9.6 GHz, but bandwidth of the chirp signals transmitted is a maximum of 100 MHz. Therefore, there is a dispersion effect during transmission. The length of coaxial l is designed to delay phase of 45° on $f_c = 9.6$ GHz, i.e., $2\pi f_c/c \cdot l = \pi/4$. Thus, the phase error caused by $\Delta f = 100$ MHz bandwidth can be expressed as

$$\Delta\varphi = 2\pi\Delta f/c \cdot l \approx 0.01 \cdot \pi/4 \approx 0.47^\circ. \tag{15}$$

The phase error is small enough that it can be ignored, which can be verified from the near-field maps in Section III-B.

B. Near-Field Maps

In order to verify that the vortex wave was generated correctly, near-field maps of the elaborate antennas were measured first. The transmitting antennas were excited vortex beams of $L = 0, 1$, and 2 modes, respectively. On the receiving plane, a probe antenna placed at $D = 1.6$ m distance from the TX, moved along a 0.8 m $\times$ 0.8 m rectangle area, whose center was right on axis of the vortex beams, with a resolution of 4 mm.

The experimental results are reported in Fig. 5. Not surprisingly, the measured intensity and phase distributions are in good agreement with vortex characteristics described in [11]. It con-

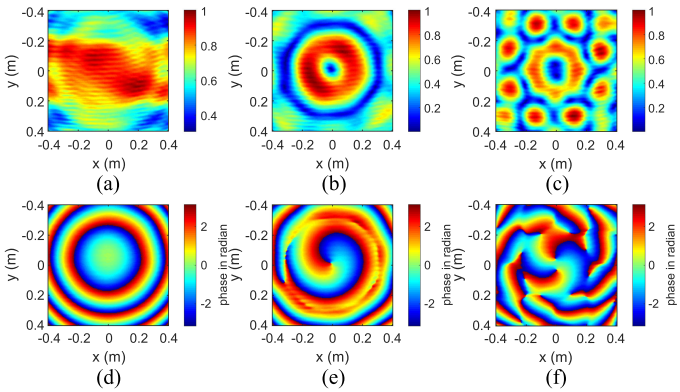

Fig. 5. Normalized magnitude (top row) and phase (bottom row) of near electric field measured by the probe antenna, which represents $L = 0, 1$, and 2-modes from left to right. (a) Magnitude, CA, L = 0. (b) Magnitude, IA, L = 1. (c) Magnitude, OA, L = 2. (d) Phase, CA, L = 0. (e) Phase, IA, L = 1. (f) Phase, OA, L = 2.

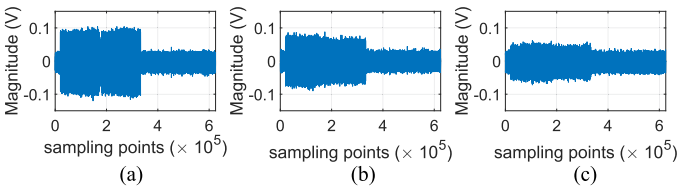

Fig. 6. One pulse from the chirp signals displayed on the oscilloscope. (a)–(c) Represents signal received from CA ($L = 0$), IA ($L = 1$), and OA ($L = 2$), respectively.

firms that the TX successfully generated vortex EM wave in near-field area. From the results, we can again verify the basic properties of the vortex beam, i.e., the helical phase wavefront and the increasing singularity at the center of beams.

C. Chirp Signal Transmission Experiment

A novel experiment, chirp signals transmission based on OAM multiplexing, was performed to demonstrate the ability to multiplex. Three different chirp signals, carrying different information (actually different FM rates, i.e., K_0, K_1, and K_2) with a 50% duty cycle but the same carrier frequency, were generated, multiplexed based on different OAM modes ($L = 0, 1$, and 2), and radiated to the free space via TX simultaneously. The RX was placed 1.6 m away from the TX in LOS and carefully aligned, because a slight misalignment (off-axis or tilt angle) will cause a very large crosstalk. Particularly in our experiment, 2.2 cm or 0.98° misalignment lead to about 10 dB interference. Then, the received signals were phase-shifted, down-converted to an intermediate frequency $f_I = 750$ MHz, and finally recorded by an oscilloscope.

Fig. 6 shows one pulse from the received chirp signals displayed on the oscilloscope. It can be seen that the signal is on 50% of the pulse period, and the amplitude of signals degrades from CA to OA. To some extent, it reflects the divergence of vortex beam with increasing L.

By using digital signal processing technology, the intermediate frequency was removed first and each chirp signal was correlated with corresponding matched filters. The results of pulse compression are shown in Fig. 7, and the maximums of all results are regarded as $\sigma_{i,j}$, where i and j represent the desired and received OAM mode, respectively. The RAC obtained

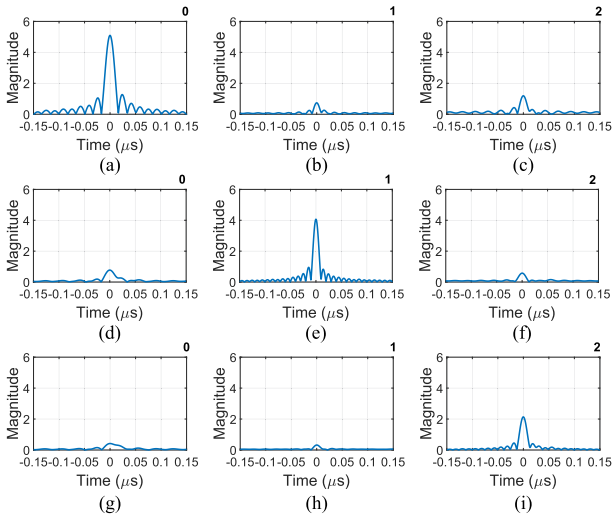

Fig. 7. Experimental pulse compression results of using different matched filters. (a)–(c), (d)–(f), and (h)–(j) indicate the signal received by the CA, IA, and OA, respectively. g_i denotes the complex conjugate of s_i. (a) CA filtered with g_0. (b) CA filtered with g_1. (c) CA filtered with g_2. (d) IA filtered with g_0. (e) IA filtered with g_1. (f) IA filtered with g_2. (g) OA filtered with g_0. (h) OA filtered with g_1. (i) OA filtered with g_2.

by the crosstalk matrix is $\mathcal{C}_{\text{exp}} = -15.0$ dB, which meets the requirements of near-field OAM multiplexing communication.

The results show that the receiving antenna can separate these multiplexing signals well without any complicated digital demultiplexing technology. This means that in the same near-field communication channel, OAM multiplexing is feasible in radio domain and does increase channel capacity without increasing signal bandwidth. However, the system is hard to apply in a practical far-field scene due to the divergence of vortex beams unless using a sufficient power [13]. On the other hand, the OAM mode number is limited by the number of antenna element of UCA because of sampling theorem [11], which greatly limits the application of OAM beams. Therefore, an elaborate metasurface to generate [20] and detect [21] vortex waves with arbitrary OAM modes is becoming promising in the future.

IV. Conclusion

In this letter, a novel experiment was proposed to show the feasibility of communication based on the radio OAM multiplexing technology, via analyzing theoretically, and carrying out in anechoic chamber. The measured two-dimensional planar near patterns show excellent vortex properties. Then, an experiment of chirp signals multiplexing on radio OAM was conducted, and the results proved that receiving antenna can retrieve the corresponding vortex mode in free-space filling with a mixed multi-OAM-mode. This means that the signals multiplexed based on radio OAM can be correctly demultiplexed in free space.

The OAM multiplexing experiment of chirp signal in this letter not only confirms the feasibility of OAM multiplexing technology in radio domain and thus increases the capacity of radio communication on the same bandwidth, but also paves the way for the application of vortex waves in radar field, especially synthetic aperture radar (SAR) field [22], [23]. In order to effectively apply the vortex wave to radar field, the scattering of vortex beams by typical targets needs further analysis and research.

REFERENCES

[1] L. Allen, M. W. Beijersbergen, R. J. C. Spreeuw, and J. P. Woerdman, "Orbital angular momentum of light and the transformation of Laguerre-Gaussian laser modes," *Phys. Rev. A*, vol. 45, pp. 8185–8189, Jun. 1992.

[2] O. Emile, C. Brousseau, J. Emile, R. Niemiec, K. Madhjoubi, and B. Thidé, "Electromagnetically induced torque on a large ring in the microwave range," *Phys. Rev. Lett.*, vol. 112, Feb. 2014, Art. no. 053 902.

[3] D. Cojoc, V. Garbin, E. Ferrari, L. Businaro, F. Romanato, and E. D. Fabrizio, "Laser trapping and micro-manipulation using optical vortices," *Microelectron. Eng.*, vol. 78/79, no. Supplement C, pp. 125–131, 2005.

[4] G. Molina-Terriza, J. P. Torres, and L. Torner, "Twisted photons," *Nature Phys.*, vol. 3, no. Supplement C, pp. 305–310, 2007.

[5] V. Ivaška and V. Kalesinskas, "Vortical electromagnetic waves with a stationary power flow," in *Proc. 18th Int. Conf. Microw., Radar Wireless Commun.*, Jun. 2010, pp. 1–4.

[6] R. C. Devlin, A. Ambrosio, N. A. Rubin, J. P. B. Mueller, and F. Capasso, "Arbitrary spin-to-orbital angular momentum conversion of light," *Science*, vol. 358, pp. 896–901, 2017.

[7] G. Gibson *et al.*, "Free-space information transfer using light beams carrying orbital angular momentum," *Opt. Express*, vol. 12, pp. 5448–5456, Nov. 2004.

[8] J. Wang *et al.*, "Terabit free-space data transmission employing orbital angular momentum multiplexing," *Nature Photon.*, vol. 6, no. 7, pp. 488–496, 2012.

[9] N. Bozinovic *et al.*, "Terabit-scale orbital angular momentum mode division multiplexing in fibers," *Science*, vol. 340, no. 6140, pp. 1545–1548, 2013.

[10] S. Mi, T. J. Wang, G. S. Jin, and C. Wang, "High-capacity quantum secure direct communication with orbital angular momentum of photons," *IEEE Photon. J.*, vol. 7, pp. 1–8, Oct. 2015, Art. no. 7600108.

[11] B. Thidé *et al.*, "Utilization of photon orbital angular momentum in the low-frequency radio domain," *Phys. Rev. Lett.*, vol. 99, Aug. 2007, Art. no. 087701.

[12] F. Tamburini, E. Mari, B. Thidé, C. Barbieri, and F. Romanato, "Experimental verification of photon angular momentum and vorticity with radio techniques," *Appl. Phys. Lett.*, vol. 99, no. 20, 2011, Art. no. 204102.

[13] F. Tamburini, E. Mari, A. Sponselli, B. Thidé, A. Bianchini, and F. Romanato, "Encoding many channels on the same frequency through radio vorticity: First experimental test," *New J. Phys.*, vol. 14, no. 3, 2012, Art. no. 033001.

[14] F. Tamburini *et al.*, "Tripling the capacity of a point-to-point radio link by using electromagnetic vortices," *Radio Sci.*, vol. 50, pp. 501–508, Jun. 2015.

[15] F. Spinello *et al.*, "Radio channel multiplexing with superpositions of opposite-sign OAM modes," *AEU—Int. J. Electron. Commun.*, vol. 70, no. 8, pp. 990–997, 2016.

[16] F. Spinello *et al.*, "Experimental near field OAM-based communication with circular patch array," Jul. 2015, arXiv:1507.06889.

[17] Y. Yan *et al.*, "High-capacity millimetre-wave communications with orbital angular momentum multiplexing," *Nature Commun.*, vol. 5, pp. 4876–4876, Sep. 2014.

[18] Y. Gong *et al.*, "Generation and transmission of OAM-carrying vortex beams using circular antenna array," *IEEE Trans. Antennas Propag.*, vol. 65, no. 6, pp. 2940–2949, Jun. 2017.

[19] J. D. Kraus and R. J. Marhefka, *Antennas*. New York, NY, USA: McGraw-Hill, Dec. 1988.

[20] M. L. N. Chen, L. J. Jiang, and W. E. I. Sha, "Ultrathin complementary metasurface for orbital angular momentum generation at microwave frequencies," *IEEE Trans. Antennas Propag.*, vol. 65, no. 1, pp. 396–400, Jan. 2017.

[21] M. L. N. Chen, L. J. Jiang, and W. E. I. Sha, "Detection of orbital angular momentum with metasurface at microwave band," *IEEE Antennas Wireless Propag. Lett.*, vol. 17, no. 1, pp. 110–113, Jan. 2018.

[22] T. Yuan, H. Wang, Y. Cheng, and Y. Qin, "Electromagnetic vortex-based radar imaging using a single receiving antenna: Theory and experimental results," *Sensors*, vol. 17, no. 3, 2017, Art. no. 630.

[23] X. Bu, Z. Zhang, L. Chen, X. Liang, H. Tang, and X. Wang, "Implementation of vortex electromagnetic waves high-resolution synthetic aperture radar imaging," *IEEE Antennas Wireless Propag. Lett.*, vol. 17, no. 5, pp. 764–767, May 2018.